W-Band Investigation of Material Parameters, SAR Distribution, and Thermal Response in Human Tissue

Frank Gustrau and Achim Bahr

***Abstract*—There are new applications in the automotive industry that make use of electromagnetic fields in the centimeter/millimeter-wave range, e.g., radar systems for adaptive cruise control. In this frequency range, only few data are available from the point of human safety and dosimetry. This investigation is divided into three parts. First, the W-band dielectric properties of different biological tissues are determined. Afterwards the electromagnetic field in the human eye and skin is simulated for plane-wave exposure. An analytical method is used to investigate the specific absorption rate (SAR) inside a layered model of the human skin between 3–100 GHz. Furthermore, the SAR inside a detailed model of the human eye is investigated numerically by the finite-difference time-domain method for a frequency of 77 GHz. Maximum local SAR values of 27.2 W/kg in skin tissue and 45.1 W/kg in eye tissue are found for 77 GHz and an incident power density of 1 mW/cm^2. In the third part of this investigation, the temperature changes of superficial tissue caused by millimeter-wave irradiation are measured by a thermal infrared imaging system. The exposure setup is based on a horn antenna with a Gunn oscillator operating at 15.8-dBm output power. The measurements showed a maximum temperature increase of 0.7 °C for a power density of 10 mW/cm^2 and less than 0.1 °C for 1 mW/cm^2, both in human skin (*in vivo*), as well as in porcine eye (*in vitro*). The comparison of the temperature measurements with a thermal bio-heat-transfer simulation of a layered skin model showed a good agreement.**

***Index Terms*—Basic restrictions, bio-heat-transfer equation, biological tissues, dielectric properties, dosimetry, finite-difference time-domain (FDTD) method, finite-element method (FEM), numerical simulation, safety guidelines, thermal imaging system, W-band.**

I. Introduction

THERE ARE new applications in the automotive industry that make use of electromagnetic fields in the centimeter/millimeter-wave range, e.g., radar systems for adaptive cruise control [8].

In this frequency range, the primary biological effect of electromagnetic fields is the heating of tissue resulting from the absorption of electromagnetic energy [22]. Consequently, the limits in safety guidelines and standards are based on the well-known thermal effect and fixed in order to avoid thermal damage of tissue [2], [13], [22]. The relevant macroscopic measure, which links the electromagnetic field with the thermal response inside the biological tissue, is the specific absorption rate (SAR). The SAR represents a local heat source [21]. According to the International Commission on Non-Ionizing Radiation Protection (ICNIRP) guidelines [22] and the European Council Recommendation [13], the basic restriction for frequencies below 10 GHz is the SAR, between 10–100 GHz, the basic restriction is the power density S. In the ANSI C95.1 Standard [2], the SAR limit is restricted to frequencies below 6 GHz. Table I lists the relevant SAR and power density limits in the frequency range from 3 up to 100 GHz for exposure of the human head and trunk. In the standards, different averaging masses for the SAR, as well as different averaging areas for the power density, have to be taken into account.

TABLE I
SAR AND POWER DENSITY LIMITS FOR NONOCCUPATIONAL EXPOSURE IN THE FREQUENCY RANGE FROM 3 UP TO 100 GHz IN DIFFERENT STANDARDS FOR EXPOSURE OF THE HUMAN HEAD AND TRUNK: ANSI C95.1 [2], EUROPEAN COUNCIL RECOMMENDATION [13], AND ICNIRP GUIDELINES [22] (*AREA EQUIVALENT TO THE CROSS SECTION OF THE HUMAN BODY)

Standard	*SAR* [W/kg]	Avg. mass for SAR	*S* [mW/cm^2]	Area [cm^2]
ANSI	1.6 (f<6 GHz)	1 g	10	*
EC	2 (f<10 GHz)	10 g	1	—
ICNIRP	2 (f<10 GHz)	10 g	1	20

In the frequency range of interest, the penetration depth of the electromagnetic wave inside the human tissue is low, and significant heating occurs in the superficial regions of the body only. Therefore, two parts of the body are of special interest, i.e., the skin and eye. The eye is particularly sensitive to heating because of its lack of blood perfusion [6], [28].

The investigation presented in this paper is divided into three parts. First, the dielectric properties of the relevant biological tissues are measured in order to provide reliable data for the assessment of the SAR distribution inside the human tissue. The results are compared with the well-established and widely used parametric model of Gabriel *et al.* [18], which allows the calculation of different biological tissues in the frequency range from 10 Hz to 100 GHz. In our investigation, the following tissues are measured in the frequency range from 75 up to 100 GHz: fat, muscle, skin (dermis), cornea, lens, liquid from the camera anterior, retina, sclera, vitreous humor.

Next, the SAR distribution is determined inside the human skin and eye by means of numerical calculations. The incident electromagnetic field is represented by a homogeneous plane wave. Skin tissue is modeled by a four-layer structure and the

Manuscript received October 25, 2001; revised November 12, 2001. This work was supported by the German Research Association for Radio Applications (Forschungsgemeinschaft Funk e.V. Bonn, Germany).

The authors are with the IMST GmbH, D-47475 Kamp-Lintfort, Germany (email: contact@imst.de).

Digital Object Identifier 10.1109/TMTT.2002.803445.

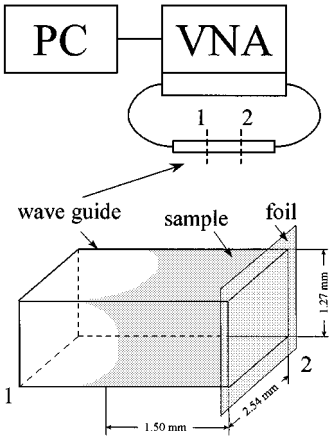

Fig. 1. Tissue sample inside the waveguide and principle setup.

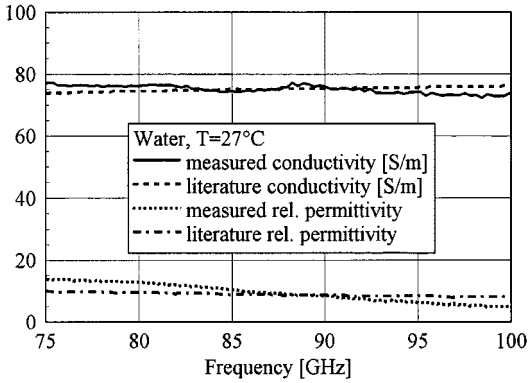

Fig. 2. Comparison of measured dielectric properties of water and theoretical properties.

electromagnetic field inside the tissue is described by an analytical model. In order to assess the field inside the human eye, a detailed model for a finite-difference time-domain (FDTD) analysis is developed. In both cases, the maximum local SAR, as well as averaged values for the SAR, are determined.

Finally, the thermal response of millimeter-wave irradiation at 77 GHz is analyzed. This investigation includes the measurement of human skin and porcine eye surface temperature *in vivo* and *in vitro*, respectively, as well as thermal simulations of the temperature inside the human skin. The tissue is irradiated with a demonstrator of a radar device, operating at 77 GHz in continuous wave (CW) mode. The superficial temperature change caused by the irradiation is recorded by an infrared thermal imaging system. The measurement results are compared with thermal simulations based on the bio-heat-transfer equation [21]. The calculated SAR inside the skin model is transferred to the thermal model and considered as a local heat source.

II. Methods

A. Measurement of Dielectric Parameters

Investigations of the dielectric properties of biological tissues have been presented in the literature for over 40 years (e.g., [11], [16], and [29]). The results are obtained by measurements of animal and human tissue in the frequency range up to 90 GHz [12].

In the upper frequency range, only few data are available. Therefore, in this investigation, the dielectric properties of different human tissues in the frequency range from 75 to 100 GHz are measured. The measurements are carried out using the measurement system WR 10 from Damaskos Inc., Concordville, PA, with a rectangular W-band waveguide. The waveguide is partially filled with a small sample of the biological tissue and connected to a vector network analyzer (VNA) (see Fig. 1). The relative permittivity and conductivity are calculated from the measured transmission coefficients. The sample has dimensions of 2.54 mm $\times$ 1.27 mm $\times$ 1.5 mm (width $\times$ height $\times$ length) for nonliquid biological tissues. For liquid material, one end of the sample is attached to a foil. At the other end, the exact shape of the sample is unknown because of the surface tension of the liquid material. A first study has shown that this phenomenon results in a reduction of the effective length of the sample with respect to its transmission characteristics and, therefore, has to be considered for the calculation of the dielectric properties. However, in practice, this effective length cannot be determined. In order to minimize the effect of surface tension, we soaked a piece of cotton wool with the liquid material. The cotton wool has no significant effect on the calculated dielectric properties. Fig. 2 visualizes a comparison of the measurement results for water using this procedure and theoretical data from literature [11], [18]. In this case, the original length of the sample is used for the calculation of the dielectric properties. The temperature of the sample is $T = 27$ °C. This comparison shows a reasonable agreement between measurement and theory.

The following tissues are measured at 27 °C and 37 °C: fat, muscle, skin (dermis). Since heating of such a small liquid sample causes evaporation, the eye tissues are only measured at 27 °C: cornea, lens, liquid from the camera interior, retina, sclera, vitreous humor.

B. Analytical Method and Model of the Human Skin

The skin of an adult man covers approximately 2 m^2 and has a thickness between 1.5–4 mm. Underneath, a fat layer (tela subcutanea) is situated, which is located above muscle tissue. The epidermis is the outer part of the skin. It is cornified, without vessels, multilayered, and normally dry. The dermis, which represents the rest of the human skin, except the fat layer, is the wet skin region. The layered model of the human skin is shown in Fig. 3.

Since the penetration depth of electromagnetic fields in the human body is very small in the frequency range of interest, the electromagnetic field can be locally described by a plane wave. Therefore, the electromagnetic problem is reduced to a one-dimensional investigation of the field distribution in a layered medium. The typical thickness of the different layers is taken from the literature [14], [25]. These values are summarized in Table II together with the mass density of the layers, which are taken from [9], [15], and [23].

The analytical method used for the calculation of the electromagnetic field in layered media is taken from [4]. The reflection coefficients and transmission coefficients of multiple interfaces between the different tissues are determined for normal incidence of a linearly polarized plane wave. Introducing a phase

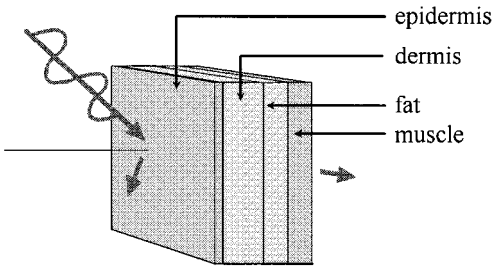

Fig. 3. Layered model of the human skin.

TABLE II
THICKNESS AND MASS DENSITY OF THE DIFFERENT LAYERS OF THE HUMAN SKIN INCLUDING TYPICAL VALUES FOR FAT AND MUSCLE (*40 mm ASSUMED IN THE SIMULATION) TISSUE

Tissue	Mass density [10^3 kg/m^3]	Thickness [mm]
epidermis	1.1	0.15
dermis	1.1	3.85
fat	0.92	10
muscle	1.04	40*

and an attenuation term upon the traveling E-field, the distribution of the electric field within the layers is calculated by superposition of the different propagating waves in the media.

The SAR distribution inside the human skin is analyzed in the frequency range from 3 to 100 GHz. The low-frequency range is included in the investigation in order to demonstrate the transition in the SAR distribution from low to high frequencies. The power density of the incident linearly polarized plane wave is 1 mW/cm^2. In this analysis, the frequency-dependent dielectric properties are taken from the parametric model in [18] since this model provides dielectric properties in closed form in the whole frequency range. For the epidermis and dermis layer, the dielectric properties of dry and wet skin are chosen, respectively.

C. FDTD Method and Model of the Human Eye

The calculations of the electromagnetic field inside the anatomical model of the human eye is carried out using the FDTD method [24], [31]. In this study, an implementation developed in [3] is used.

For the numerical investigation of the field distribution, a three-dimensional cubic voxel model of a spherical human eye is developed. The eye has a diameter of $d = 20.8$ mm and is embedded in muscle and skin tissue. Fig. 4 shows a cut plane through this voxel model with a homogeneous discretization.

The tissues of the eye are: 1) retina; 2) choroidea; 3) sclera; 4) cornea; 5) iris; 6) lens; 7) camera anterior; 8) vitreous humor; and 9) nervus opticus. The dielectric parameters are listed in Table III.

For the excitation, a normally incident plane wave with a power density of $S = 1$ mW/cm^2 and a frequency of 77 GHz is applied.

D. Thermal Measurement

For the experimental investigation of thermal effects in the human skin and in the porcine eye, a high-speed thermal image system (Thermo Tracer TH 2111, NEC San-ei Instruments Ltd., Tokyo, Japan) is used. This system is a noncontact-type infrared thermometer.

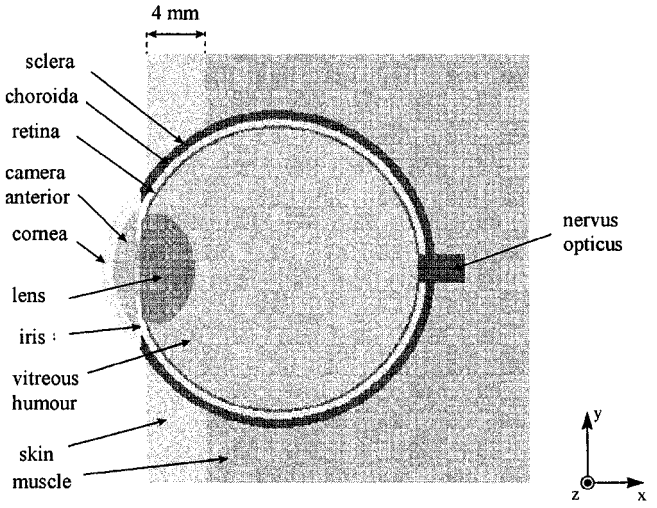

Fig. 4. FDTD model of the human eye.

TABLE III
MASS DENSITY ρ, RELATIVE PERMITTIVITY ε_r, AND CONDUCTIVITY σ OF THE TISSUES OF THE EYE MODEL AT 77 GHz (*OUR MEASUREMENT, #NO DATA AVAILABLE: PROPERTIES OF MUSCLE TISSUE USED)

Tissue	Mass density ρ [10^3 kg/m^3]	Permittivity ε_r	Conductivity σ [S/m]
camera anterior	1.006	4*	48*
choroidea	1.06	28#	106#
cornea	1.06	6*	56*
iris	1.058	28#	106#
lens	1.1	14*	30*
muscle	1.04	28*	106*
nervus opticus	1.035	28#	106#
retina	1.035	8*	54*
sclera	1.1	23*	77*
skin	1.1	12*	56*
vitreous humour	1.006	10*	41*

The detector unit of the thermal image system scans the surface of an object and collects the infrared energy by an infrared objective lens. After chopping this infrared energy with a reference temperature source, it is converted to an electrical signal using an infrared HgCdTe detector. The relation between the radiated energy and temperature is given by the well-known Planck radiation law. The infrared detector remains cooled to -196 °C by liquid nitrogen and is capable of converting infrared energy with high sensitivity.

The main performance specifications of the system are as follows: temperature resolution: 0.1 °C (for blackbody at 30 °C), 0.02 °C (in S/N improvement mode, for blackbody at 30 °C).

For exposure, a generator based on a Gunn-diode oscillator with an output power up to 38 mW is used. The frequency of the CW signal is 77 GHz and the size aperture of the rectangular horn antenna is 1.5 cm × 1.1 cm. The gain of the horn antenna is $G = 20$ dBi. An estimation of the power density yields $S = 1$ mW/cm^2 at a distance of $d = 17.3$ cm in front of the aperture and a power density of 10 mW/cm^2 at a distance of $d = 5.5$ cm.

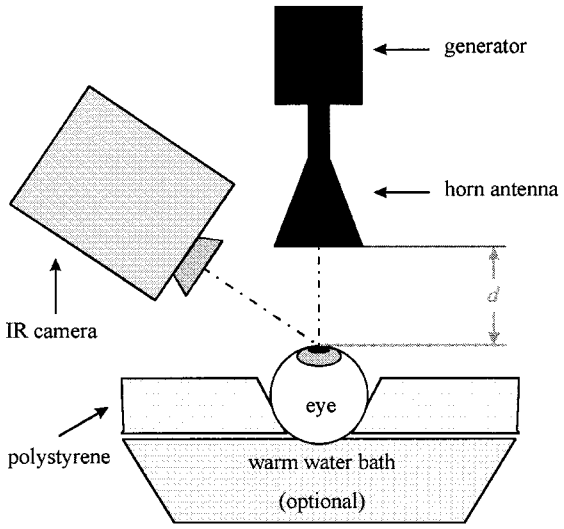

Fig. 5. Block diagram of the experimental setup for *in vitro* eye temperature measurement.

For the exposure of human skin, the antenna is oriented to the forearm of two volunteers and the time-dependent temperature field in the region of interest is recorded by the thermal image system. All experiments are carried out in an anechoic chamber.

Before the measurement, the volunteers have a time to rest in order to wait for thermal equilibrium in the human forearm. The thermophysiological response of the skin *in vivo* is determined for different distances d between the skin and exposure system. The power was set to the maximum of $P = 38$ mW for all measurements. The ambient temperature during the different measurements is between 21 °C and 22 °C, but is constant ($\pm$0.1 °C) for each measurement. The relative humidity of air is between 50%–60%. There is essentially no air motion in the laboratory.

Due to small motion artifacts, the resolution of the thermal image system, and slight changes in the ambient conditions, the accuracy of the measurement is estimated to be approximately 0.1 °C–0.2 °C in the region of interest.

The experimental setup for the thermal investigation of porcine eyes is similar to that for the investigation of skin temperature change. The schematics of the experimental setup are shown in Fig. 5. The eye is inserted into a polystyrene layer and positioned over a warm water bath ($T_{\text{water}} = 37$ °C) in order to consider the core temperature behind the eye. The experiment is repeated without the warm water bath in order to determine the influence of the physiological temperature on thermal performance.

E. Thermal Simulation

In 1948, Pennes proposed a mathematical model for heat-transfer processes in blood-perfused tissue. Although more complex models for heat-transfer processes have been developed, Pennes' approach has been refined and is still being used today [7]. Pennes' model describes the effect of blood flow on tissue temperature on a continuum basis. Therefore, a heat source/sink term is introduced in the heat equation

$$\rho c_p \frac{\partial T}{\partial t} = \nabla(\lambda \nabla T) + \rho(MR + SAR) + \xi \rho_b c_b (T_a - T). \tag{1}$$

The parameters of this equation are: 1) ρ mass density of tissue; 2) c_p specific heat capacity of tissue; 3) λ thermal conductivity; 4) MR heat generation rate according to metabolic processes (= metabolic rate); 5) ξ perfusion rate; 6) ρ_b mass density of blood; 7) c_b specific heat capacity of tissue; 8) T_a arterial temperature; and 9) SAR.

On the surface of the body, Cauchy boundary conditions are applied in order to account for the heat loss to the environment

$$\mathbf{n}^T \cdot \dot{\mathbf{q}} = \alpha(T - T_u) \tag{2}$$

where α is the heat-transfer coefficient, $\dot{\mathbf{q}}$ is the heat flow, T_u is the ambient temperature, and $\mathbf{n}$ is the outward unit normal vector. The heat-transfer coefficient α considers the four heat-loss mechanisms, i.e., radiation, convection, conduction, and evaporation. The differential equation with initial and boundary conditions is solved using a finite-element method (FEM)-based program described in [21].

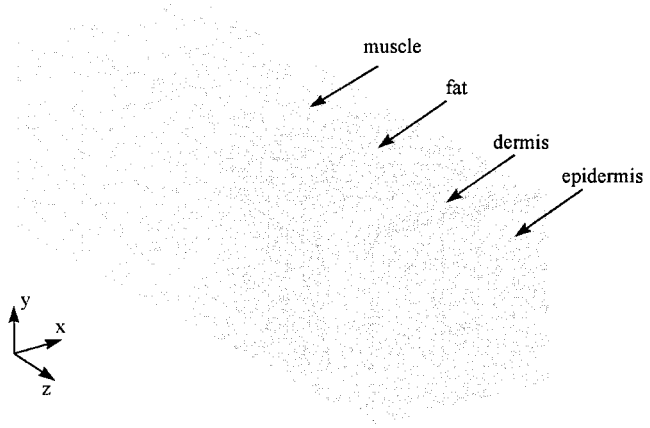

Fig. 6. Finite-element model for the thermal simulation of skin tissue.

TABLE IV
THERMAL PROPERTIES OF SKIN TISSUE

Parameter	Epidermis	Dermis	Fat	Muscle
c_p [J/(kg·K)]	3350	3350	3350	3350
λ [W/(m·K)]	0.5	0.5	0.5	0.5
MR [W/m³]	0	200	200	200
ξ [m³/(s·m³)]	0	2.43e-4	2.43e-4	1.0e4
α [W/(m²·K)]	12	0	0	0

Fig. 6 shows the finite-element model for the one-dimensional analysis of the heat-transfer processes in the skin. The thickness of the layers is chosen according to Table II. The SAR of the analytical approach is scaled to an incident power density of $S = 10\,\text{mW/cm}^2$ (according to [2]) and applied to the thermal model.

Table IV shows the thermal parameters of the three different tissues taken from [1] and [30]. The high perfusion rate of muscle identifies the isothermal core region of the body. The

TABLE V
MEASURED RELATIVE PERMITTIVITY ε_r AND CONDUCTIVITY σ OF PORCINE TISSUE IN THE FREQUENCY RANGE FROM 75 UP TO 100 GHz (±STANDARD DEVIATION). (IN BRACKETS: RESULTS FROM THE PARAMETRIC MODEL OF GABRIEL IF AVAILABLE)

Tissue	Permittivity ε_r	Conductivity σ [S/m]
fat (27 °C)	10±1 [4.0]	56±2 [9.5]
fat (37 °C)	10±1 [4.0]	57±2 [9.5]
muscle (27 °C)	20±3 [10.5]	104±6 [57.9]
muscle (37 °C)	28±3 [10.5]	106±6 [57.9]
skin (dermis) (27 °C)	12±2 [8.5]	56±2 [42.9]
skin (dermis) (37 °C)	15±2 [8.5]	54±2 [42.9]
camera anterior (27 °C)	4±1 [—]	48±2 [—]
cornea (27 °C)	6±1 [9.6]	56±2 [53.1]
lens (27 °C)	14±1 [8.8]	30±2 [45.5]
retina (27 °C)	8±1 [—]	54±1 [—]
sclera (27 °C)	23±2 [9.74]	77±4 [54.6]
vitreous humour (27 °C)	10±1 [8.9]	41±1 [75.0]

additional parameters are: 1) $T_a = 36$ °C; 2) $c_b = 3350$ J/(kg · K); and 3) $\rho_b = 1000$ kg/m^3.

Thermoregulatory effector mechanisms, i.e., changes in physiological parameters like perfusion rate caused by the thermal impact, are negligible and, therefore, not considered in this investigation.

III. RESULTS AND DISCUSSION

A. Dielectric Properties of Tissue

As demonstrated by the verification with pure water, the accuracy of the measurement procedure is very good for electrical conductivity. For relative permittivity, the accuracy is less good and shows a stronger gradient than the theoretical curve. In the frequency range from 75 up to 100 GHz, the tissues show small changes in the dielectric properties compared with the accuracy of the measurement procedure. Therefore, only one value is given for the relative permittivity and conductivity in the frequency range of interest. Thirty-five measurement points are taken and the average value as well as the standard deviation have been determined. The values are listed in Table V. The skin tissues are measured at 27 °C and 37 °C. The eye tissues are measured at room temperature 27 °C only, since the handling of eye tissues at higher temperatures is difficult due to evaporation of water. The tissue samples are prepared by biologists: the appropriate tissue is excised from a freshly killed pig, the materials are homogenized and filled into the waveguide. Finally, the length of the probe in the waveguide is determined using a pipet of a patch–clamp system.

The dielectric properties of biological tissue are affected by some factors, which are: 1) temperature (temperature coefficient <2% per °C [26]); 2) natural variability of tissue (approximately 5% [19]); 3) aspecies (e.g., porcine versus human) (about 5%). "The variation in tissue properties within a species may well exceed variations between species" [19]; 4) anisotropy of muscle tissue is an important issue at low frequencies. Above 1 MHz muscle tissue becomes essentially isotropic [11]; and 5) only small changes following death above 1 MHz are reported by [11].

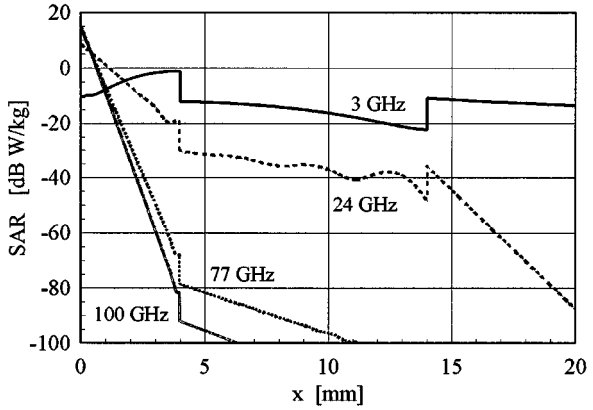

Fig. 7. Distribution of the SAR for 3, 24, 77, and 100 GHz inside the model of the human skin for an incident power density of 1 mW/cm^2.

TABLE VI
MAXIMUM SAR, 1- AND 10-g-AVERAGED SAR AT DIFFERENT FREQUENCIES FOR AN INCIDENT POWER DENSITY OF 1 mW/cm^2

f [GHz]	SAR_{max} [W/kg]	SAR_{1g} [W/kg]	SAR_{10g} [W/kg]
3	0.098	0.20	0.11
6	0.80	0.24	0.14
24	7.74	0.42	0.20
77	27.2	0.58	0.27
100	33.9	0.62	0.29

The results show significant deviations from the data reported by Gabriel *et al.* [18], especially for fat tissue, which shows a considerably higher conductivity than predicted by Gabriel *et al.* However, Gabriel and Gabriel demonstrated in the literature survey [19] that the dielectric properties of fat tissue show a great span up to a factor of ten between minimum and maximum reported values. Furthermore, above 20 GHz, Gabriel and Gabriel's parametric model is based on very few experimental data.

B. SAR Results in Skin Tissue

The results of the SAR calculation inside the human skin for an incident power density of 1 mW/cm^2 are shown in Fig. 7 for a frequency of 77 and 100 GHz. In order to show the transition from low to high frequencies, the SAR distribution for frequencies of 3 and 24 GHz is included in the graphical plot. With increasing frequency, the penetration depth of the electromagnetic wave decreases and the absorption of electromagnetic energy becomes more and more superficial.

The maximum local SAR values as well as the 1- and 10-g-averaged SAR values according to the different safety standards are listed in Table VI. In the W-band, the electromagnetic field is nearly totally absorbed in the skin (dermis and epidermis) and the maximum SAR occurs on the surface of the skin. The inhomogeneous distribution shows that the averaging of SAR approximately 1 or 10 g no longer results in a meaningful measure.

The results show a good agreement with the literature. For a frequency of 100 GHz, Gandhi and Riazi [20] predicted a $\mathrm{SAR}_{\max} = 41.6$ W/kg, compared to 33.9 W/kg in our investigation.

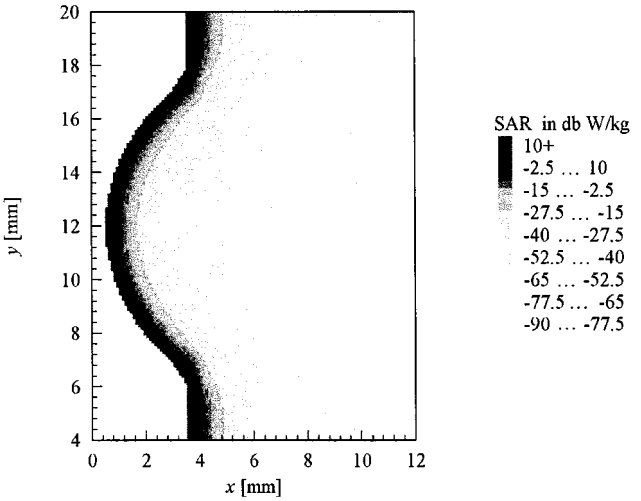

Fig. 8. SAR distribution in the xy-plane. The model of the human eye for an incident power density of 1 mW/cm^2 at 77 GHz.

TABLE VII
MAXIMUM LOCAL SAR IN THE DIFFERENT TISSUES OF THE EYE MODEL FOR PLANE-WAVE EXCITATION (NORMAL INCIDENCE) WITH 1 mW/cm^2

Tissue	SAR_{max} [W/kg]
camera anterior	0.366
Choroidea	1.71
Cornea	45.1
Iris	0.921
Lens	$1.58 \cdot 10^{-3}$
Muscle	$2.32 \cdot 10^{-5}$
nervus opticus	$< 1 \cdot 10^{-6}$
Retina	$4.96 \cdot 10^{-2}$
Sclera	32.5
skin	32.2
vitreous humour	$1.10 \cdot 10^{-2}$

C. SAR Results in Eye Tissue

Fig. 8 shows the distribution of the SAR in a sagittal plane of the eye for an incident power density of 1 mW/cm^2 at a frequency of 77 GHz. Due to the strong attenuation of the wave inside the eye tissues, most of the power is absorbed in the superficial tissues.

In Table VII, the maximum values of the SAR are listed for the different tissues of the model. The 1-g averaged SAR value is 0.66 W/kg. The maximum SAR value occurs in the cornea. The maximum SAR in the cornea (45.1 W/kg) is slightly higher than in the skin (27.2 W/kg), which might be a result of the higher conductivity of cornea tissue compared with dry skin (epidermis).

In order to analyze how variations in the dielectric parameters affect the maximum surface SAR, a one-dimensional investigation is performed at 77 GHz. A plane wave hits a half-space made of cornea tissue. The surface SAR at the air–cornea interface is calculated from the transmission coefficient. The dielectric parameters of tissue are changed and the impact on the surface SAR is analyzed. The dielectric parameters in the simulation are relative permittivity $= 6$ and conductivity $= 56$ S/m. Reducing the relative permittivity by 50% increases the surface SAR by 8.1%. Increasing the relative permittivity by 50% decreases the surface SAR by 9.0%. Reducing the conductivity by 50% reduces the surface SAR by 29%. Increasing the relative permittivity by 50% increases the surface SAR by 13.4%. Therefore, the conductivity is the more crucial value.

TABLE VIII
SUPERFICIAL TEMPERATURE CHANGES (±STANDARD DEVIATION) IN SKIN AND EYE TISSUE FOR AN INCIDENT POWER DENSITY OF 1 AND 10 mW/cm^2 AT 77 GHz

S [mW/cm²]	human skin (*in-vivo*)	porcine eye (*in-vitro*)
1	< 0.1 °C	< 0.1 °C
10	0.7±0.15 °C	0.7±0.11 °C

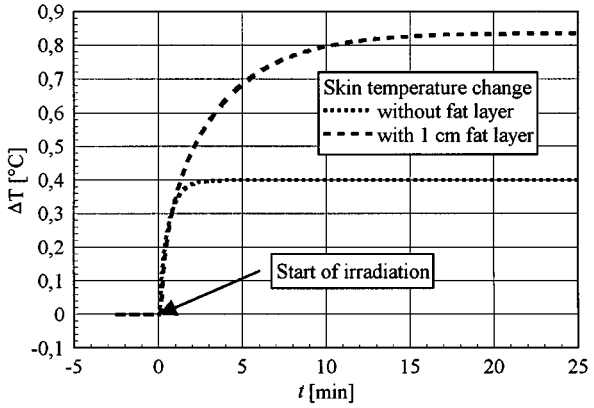

Fig. 9. Results of the thermal simulation of superficial temperature change in skin for an incident power density of 10 mW/cm^2 at 77 GHz. The simulation is carried out with and without a fat layer.

D. Measurements of Skin and Eye Temperature Change

In Table VIII, the measured temperature changes of superficial tissue are listed for a power density of 1 and 10 mW/cm^2. Five volunteers as well as five eyes of a pig are investigated. No significant differences in the temperature change between the eye at an ambient temperature and the eye heated by a warm water bath (37 °C) are observed in the investigation.

E. Simulation of Skin Temperature Change

Fig. 9 shows the time plot of the superficial temperature change in the layered model.

The simulation is carried out with and without a fat layer. It turns out that the isolation of the fat layer influences both the amplitude and the dynamic of the heat-balance process. In the simulation with a fat layer, a steady-state temperature change of $\Delta T = 0.84$ °C is achieved after 15 min of exposure; in the simulation without a fat layer, a temperature rise of $\Delta T = 0.4$ °C is achieved after 3 min. The simulation results for a power density of $S = 10$ mW/cm^2 are compared with the measurement of skin temperature changes for a distance $d = 5.5$ cm. The measurement data shows a temperature change of $\Delta T \approx 0.7$ °C. In view of the natural variability of measurement data due to inter- and intra-individual differences of the biological system, and in view of the reduced complexity of the model, which considers only one-dimensional heat transfer, the results of the thermal measurements and simulations provide consistent results for the

assessment of thermal effects of electromagnetic irradiation at 77 GHz.

IV. Conclusions

In this paper, dielectric properties of tissues, penetration of electromagnetic fields inside the human body, and resulting thermal effects on the surface of the body have been investigated.

The investigation of the human skin has been carried out using material parameters from the parametric model of Gabriel *et al.* because it provides a closed form over the entire frequency range and allows to study the transition of the SAR distribution from lower frequencies (3 GHz) up to 100 GHz. Of course, the choice of dielectric properties influences the computational results. This effect can be estimated by the transmission coefficient of the boundary air skin. Due to the strong absorption of the electromagnetic fields in superficial tissue, the averaged values for higher frequencies are determined mainly by the parameters of the first layer of the model including the reflection coefficient of the boundary air skin. The simulations showed that the highest SAR value occurs at the surface of the skin for a frequency of 100 GHz.

The human eye is modeled as a rotary body with the above-mentioned tissues. The calculation is carried out using the FDTD method at a frequency of 77 GHz and plane-wave exposure with a power density of 1 mW/cm^2. At this frequency, the calculations of the three-dimensional model of the human eye and the layered skin model show similar results. In both cases, maximum absorption occurs in superficial tissues and the maximum local SAR values are comparable: for the layered model of skin, the maximum local SAR value is 27 W/kg and, for the model of the human eye, the local SAR value is 45 W/kg in the cornea tissue.

The analysis of the SAR reveals a high attenuation and low penetration depth of the electromagnetic wave inside the skin and eye in the W-band. The SAR distribution is very inhomogeneous. The highest values of the SAR are found in the outer layers of the human skin because of the strong increase of the losses in the human skin as a function of frequency. For 77 GHz, a decrease of the SAR of nearly ten decades is observed from the epidermis layer to the fat layer. For a power density of 1 mW/cm^2, the strong losses yield a maximum SAR of 34 W/kg at 100 GHz and 27 W/kg at 77 GHz. This allows the conclusion that, in the W-band, it is not necessary to model the whole eye in great detail, but it is sufficient to consider its surface region.

For the investigation of thermal effects, an infrared thermography system is used. A radiation source with a horn antenna is oriented toward the skin of the forearm of two volunteers and toward a porcine eye (*in vitro*). The measured temperature changes in the skin and eye are in the order of 0.7 °C for a power density of 10 mW/cm^2, and less than 0.1 °C for 1 mW/cm^2. The temperature changes are beneath the warmth sensation thresholds of the volunteers.

Finally, the calculated distribution of the SAR is imported in a thermal model. The thermal calculations are based on the FEM. Two canonical skin models are analyzed, i.e., a layered model with and without a fat layer. The optional fat layer leads to an isolation between the isothermal core and the shell of the body. Hence, it influenced the dynamic and amplitude of the heat-balance process. The simulations show temperature changes in the same order of magnitude as the measurement: for a power density of 10 mW/cm^2, the temperature rise is approximately 0.7 °C in the measurement, and between 0.4 °C–0.84 °C in the simulation.

References

[1] J. Aschoff, B. Günther, and K. Kramer, "Energiehaushalt und Temperaturregulation," in *Physiologie des Menschen*, Gauer, Kramer, and Jung, Eds. Munich, Germany: Urban und Schwarzenberg, 1971, vol. 2, pp. 43–116.

[2] *IEEE Standard for Safety Levels with Respect to Human Exposure to Radio Frequency Electromagnetic Fields, 3 kHz to 300 GHz*, ANSI Standard C95.1, 1992.

[3] A. Bahr, "Zeitbereichsverfahren zur elektromagnetischen Analyse von Systemen der modernen Kommunikationstechnik," Ph.D. dissertation, Dept. Elect. Eng., Univ. Duisburg, Duisburg, Germany, 1997.

[4] C. A. Balanis, *Advanced Engineering Electromagnetics*. New York: Wiley, 1989, pp. 180–253.

[5] P. Bernardi, M. Cavagnaro, and S. Pisa, "Evaluation of the power absorbed in human eyes exposed to millimeter waves," in *Int. Electromagnetic Compatibility Symp.*, vol. 1, Rome, Italy, Sept. 1996, pp. 194–199.

[6] P. Bernardi, M. Cavagnaro, S. Pisa, and E. Piuzzi, "SAR distribution and temperature increase in an anatomical model of the human eye exposed to the field radiated by the user antenna in a wireless LAN," *IEEE Trans. Microwave Theory Tech.*, vol. 46, pp. 2074–2082, Dec. 1998.

[7] Y. I. Cho, J. P. Hartnett, and T. F. Irvine, Eds., *Bioengineering Heat Transfer, Advances in Heat Transfer*. San Diego, CA: Academic, 1992, vol. 22.

[8] "Biomedical effects of electromagnetic fields," presented at the COST 244bis Emerging Technol. Workshop, Southampton, UK, Nov. 6–7, 1999.

[9] P. J. Dimbylow, "The calculation of induced currents and absorbed power in a realistic, heterogeneous model of the lower leg for applied electric fields from 60 Hz to 30 MHz," *Phys. Med. Biol.*, vol. 33, pp. 1453–1468, 1988.

[10] P. J. Dimbylow and O. P. Gandhi, "Finite-difference time-domain calculations of SAR in a realistic heterogeneous model of the head for plane-wave exposure form 600 MHz to 3 GHz," *Phys. Med. Biol.*, vol. 36, pp. 1075–1089, 1991.

[11] F. A. Duck, *Physical Properties of Tissue: A Comprehensive Reference Book*. London, U.K.: Academic, 1990.

[12] J. Edrich and P. C. Hardee, "Complex permittivity and penetration depth of muscle and fat tissues between 40 and 90 GHz," *IEEE Trans. Microwave Theory Tech.*, vol. MTT-24, pp. 273–275, May 1976.

[13] "1999/519/EC: Council recommendation of 12 July 1999 on the limitation of exposure of the general public to electromagnetic fields (0 Hz to 300 GHz)," *Official J.*, vol. L 199, pp. 0059–0070, 1999.

[14] K. Fleischhauer, J. Staubesand, and W. Zenker, *Benninghoff Anatomie 3*. Munich, Germany: Urban and Schwarzenberg, 1985.

[15] O. Fujiwara and A. Kato, "Computation of SAR inside eyeball for 1.5 GHz microwave exposure using finite-difference time-domain technique," *IEICE Trans. Commun.*, vol. E77-B, no. 6, pp. 732–737, 1994.

[16] S. Gabriel, R. W. Lau, and C. Gabriel, "The dielectric properties of biological tissue: I. Literature survey," *Phys. Med. Biol.*, vol. 41, pp. 2231–2249, 1996.

[17] ——, "The dielectric properties of biological tissue: II. Measurements in the frequency range 10 Hz to 20 GHz," *Phys. Med. Biol.*, vol. 41, pp. 2251–2269, 1996.

[18] ——, "The dielectric properties of biological tissue: III. Parametric models for the dielectric spectrum of tissues," *Phys. Med. Biol.*, vol. 41, pp. 2271–2293, 1996.

[19] C. Gabriel and S. Gabriel, "Compilation of the dielectric properties of body tissue at RF and microwave frequencies," Brooks Air Force Base, San Antonio, TX, Rep. AL/OE-TR-1996-0037. [Online]. Available: http://www.brooks.af.mil/AFRL/HED/hedr/reports/home.html, 1996.

[20] O. P. Gandhi and A. Riazi, "Absorption of millimeter waves by human beings and its biological implications," *IEEE Trans. Microwave Theory Tech.*, vol. IEEE MTT-34, pp. 228–235, Feb. 1986.

[21] F. Gustrau and H. Ermert, "Numerical simulation and experimental investigation of thermal effects of RF-fields on patients during MRI," *Appl. Comput. Electromagn. Soc. J.*, vol. 16, no. 2, pp. 106–113, 2001.
[22] ICNIRP, "Guidelines for limiting exposure to time-varying electric, magnetic, and electromagnetic fields (up to 300 GHz)," *Health Phys.*, vol. 41, no. 4, pp. 449–522, 1998.
[23] ICRP, *Report of the Task Group on Reference Man.*. Oxford, U.K.: Pergamon, 1975, ICRP 23.
[24] K. S. Kunz and R. J. Luebbers, *The Finite Difference Time Domain Method for Electromagnetics*. Boca Raton, FL: CRC Press, 1993.
[25] H. Lippert, *Lehrbuch Anatomie*. Munich, Germany: Urban and Schwarzenberg, 1990, pp. 85–541.
[26] S. M. Michaelson and J. C. Lin, *Biological Effects and Health Implications of Radiofrequency Radiation*. New York: Plenum, 1987.
[27] K. E. Mokhtech, G. Y. Delisle, and A. G. Roberge, "SAR mapping within the human eye due to portable transceivers," in *IEEE Int. Electromagnetic Compatibility Symp.*, Chicago, IL, Aug. 26–30, 1994, pp. 26–30.
[28] S. W. Rosenthal, L. Birenbaum, I. T. Kaplan, W. Metlay, W. Z. Snyder, and M. M. Zaret, "Effects of 35 and 107 GHz CW microwaves on the rabbit eye," in *USNC/URSI Annu. Meeting*, Biological effects of electromagnetic waves, C. Johnson and M. L. Shore, Eds., Boulder, CO, 1976, pp. 110–128.
[29] H. P. Schwan, "Electric properties measured with alternating currents; body tissues," in *Handbook of Biological Data*, W. S. Spector, Ed. Philadelphia, PA: Saunders, 1957.
[30] J. Werner, *Regelung der menschlichen Körpertemperatur*. Berlin, Germany: W. de Gruyter, 1984.
[31] K. S. Yee, "Numerical solution of initial boundary value problems involving Maxwell's equations in isotropic media," *IEEE Trans. Antennas Propagat.*, vol. AP-14, pp. 302–307, Mar. 1966.

Frank Gustrau was born in Bochum, Germany, in 1967. He received the Dipl.-Ing. degree in electrical engineering and the Ph.D. degree from the Ruhr-University Bochum, Bochum, Germany, in 1993 and 1997, respectively.

From 1993 to 1997, he was a Research Assistant with the Institute for High-Frequency Technique, Ruhr-University Bochum, where he was involved with numerical modeling of electromagnetic irradiation of patients during magnetic resonance imaging. Since 1997, he has been a Senior Research Engineer with the IMST GmbH, Kamp-Lintfort, Germany. He has authored and coauthored several scientific publications. His research interests include numerical simulation of electromagnetic fields and thermal effects in the human body.

Dr. Gustrau was the recipient of a 1998 award presented by the German Society for EMC Technology (DEMVT) for his work on numerical simulation of induced low-frequency electromagnetic fields in the human body.

Achim Bahr was born on October 14, 1965, in Viersen, Germany. He received the Dipl.-Ing. degree in electrical engineering and the Ph.D. degree from the Gerhard-Mercator-University Duisburg, Duisburg, Germany, in 1992 and 1997, respectively. His doctoral dissertation concerned FDTD analysis of wireless communication devices.

He was a Research Engineer with the IMST GmbH, Kamp-Lintfort, Germany. Since 1997, he has been Head of the RF & Dosimetry Section, IMST. He has authored and coauthored over 40 scientific publications. His research interests include human safety in electromagnetic fields, numerical simulations, dosimetric measurements, and antennas for mobiles.